CHAPTER 3

MODELLING THE *JV* CHARACTERISTICS OF PDPP5T:[70]PCBM SOLAR CELLS

Summary

This chapter presents the simulation of the current-voltage characteristics of PDPP5T:[70]PCBM solar cells with different active layer morphologies. The charge transport and recombination data, presented in the previous chapter, are used here to model the *JV* curve of the devices. Both devices with homogeneous active layers and with coarse phase separation are modelled. In this chapter it is proven that it is possible to use a 1D drift-diffusion model to simulate bulk heterojunction devices even when the morphology of the active layer presents a considerable amount of phase separation. The advantage of using a 1D approach lies in its simplicity if compared with 2D and 3D models, which makes the calculations fast. An interpretation of the experimental data and an understanding of the physical phenomena which determine the device performance can be achieved with the approach presented here.

3.1 Introduction

The electrical properties of the PDPP5T:[70]PCBM blends presented in the previous chapter will be used here to model the JV characteristics of the solar cells. For the homogeneous layers, it is shown how the performance of the device with low [70]PCBM content is limited by the build-up of negative space charge (due to the large difference between electron and hole mobilities) and by the electric field dependency of the mobility of electrons. We prove that these effects are not present in the homogeneous blends containing a large amount of fullerene, in which the fine dispersion of donor and acceptor is guaranteed by the use of *o*DCB as a co-solvent. These latter devices are the best performing ones.

For the device with phase-separated morphology, we quantify the two different contributions to the total photocurrent of the devices, relating them to the morphological features of the active layer. The simulation of the two contributions is carried out using a 1D drift-diffusion model which consistently describes the JV characteristics of homogeneous polymer:fullerene solar cells taking into account generation and bimolecular recombination of free charge carriers, charge transport and injection, and the effect of the net carrier density on the electric field.[1] The sum of these contributions represents the total photocurrent; its agreement with the experimental data allows us to have an insight into the physics of BHJs, quantifying the effect of the presence of large [70]PCBM domains on the device performance.

With this modelling approach, we show how the experimental data can be interpreted with the aid of 1D drift-diffusion model. Compared with 2D and 3D approaches, 1D modelling has the advantage of requiring less computational effort; it is therefore appealing to extend the possibility of using it, even for morphologies presenting a certain extent of phase separation.

3.2 Drift-diffusion modelling

In this section we briefly introduce the 1D drift-diffusion model that we use in our work; then, we present a simplified picture of the active layer of a bulk heterojunction solar cell with coarse phase separation, based on AFM (Chapter 2) and transmission electron microscopy (TEM) images.[2] Finally, we use this simplified scheme to identify two different contributions to the total photocurrent, each of which will be simulated with the 1D model.

3.2.1 1D drift-diffusion model

The operation of drift-diffusion modelling is described in Section 1.7. Briefly, 1D drift-diffusion simulations can be implemented employing the metal-insulator-metal (MIM) approach. This consists in treating the blend as one intrinsic semiconductor material whose lowest unoccupied molecular orbital (LUMO) and highest occupied molecular

orbital (HOMO) energy levels correspond to the LUMO and HOMO levels of the acceptor and of the donor material, respectively. Based on this approach, a numerical simulation code was developed, the details of which can be found in Ref. 1.

3.2.2 Morphology schematization

When PDPP5T:[70]PCBM devices are prepared without adding *o*DCB as co-solvent and with a [70]PCBM concentration beyond a certain threshold (see Chapter 2), a coarse phase separation in the active layer is obtained. In Figure 2.3c and d we present AFM images of such active layers. Ref. 2 shows TEM images of PDPP5T:[70]PCBM devices prepared using the same procedure; we assume that the morphology shown there is the same of our active layers. [70]PCBM blobs appear as almost circular in the top view of the films. From the TEM image of the cross sections,[2] it is clear that the blobs do not extend over the entire thickness of the film, because a thin skin layer ($\sim$ 5 nm) of polymer-rich phase exists at the top and at the bottom. Regardless of the layer thickness, the height of the [70]PCBM domains is larger than that of the matrix phase.

We approximate the morphology of the active layer as shown in Figure 3.1a. Similar representations of the morphology can be found in the literature[3,4] The [70]PCBM blobs are represented as cylinders, all with the same radius and height, with the basis parallel to the electrodes. As the topological AFM image indicates (see Chapter 2), the thickness of the film is not uniform, but it is larger on top of the [70]PCBM aggregates. We consider the thickness of the acceptor phase (T_A) to be the value that we measured with the profilometer. The total number of blobs is defined by the volume fraction of the pure acceptor phase, that we calculate with the geometrical parameters listed in Table 3.1. At both electrodes a skin layer is incorporated. We verified that approximating the shape of the blobs to cylinders does not affect the outcome of the model in a significant way (see the next chapter).

The morphology is thus described with a few geometrical parameters: the thickness of the mixed and of the acceptor phase (T_M and T_A, respectively), the radius of the blobs R, the ratio between the surface of the cylinders and the total surface of the cell. We extract all these parameters from the analysis of AFM and TEM images. Besides the geometry, the composition of the two phases has to be defined. We assume that the blobs are constituted by pure [70]PCBM. To calculate the concentration of [70]PCBM into the mixed phase, the total volume of [70]PCBM present in the device is balanced: the sum of the volume of [70]PCBM blobs and the volume of [70]PCBM dispersed into the matrix has to be equal to the total volume of [70]PCBM into the active layer, which is known. As expected, the calculated [70]PCBM concentration into the mixed phase is lower than 28 vol% and it is smaller for the device with larger blobs.

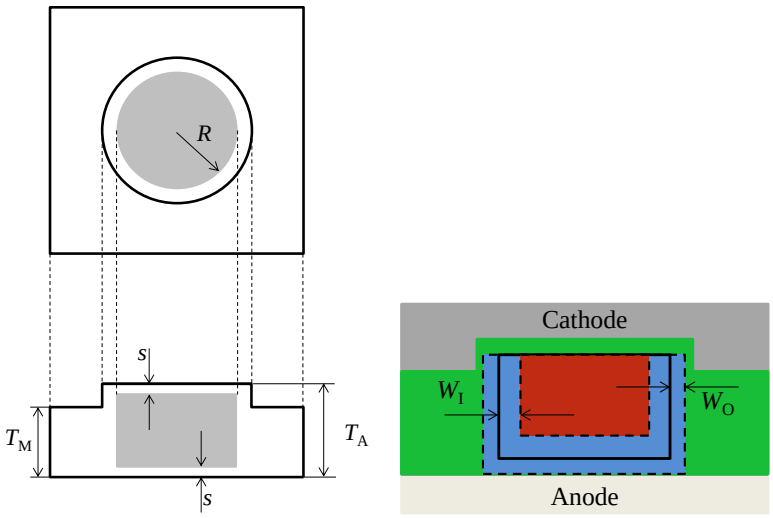

Figure 3.1: Schematic representation of the morphology of PDPP5T:[70]PCBM blends spin cast from chloroform (not to scale): a) top view and cross section. They grey area represents the [70]PCBM blob and the white area represents the mixed phase. The meaning of the symbols is explained in Table 3.1; (b) schematic representation of the regions giving rise to $J_{\text{interface}}$ (blue) and J_{mixed} (green). The red region does not contribute to the total photocurrent.

Table 3.1: Geometrical parameters for the schematized morphology of the devices made with PDPP5T:[70]PCBM 1:2 wt. ratio from chloroform solution.

Symbol	Description	Units	Thick device	Thin device
T_A	Thickness of the acceptor phase	nm	260	110
T_M	Thickness of the mixed phase	nm	200	80
R	Radius of [70]PCBM blobs	nm	220	186
s	Thickness of the skin layers	nm	5	5
$\%A$	Volume% of the acceptor phase	%	47.56	44.39
C_M	Volume% of [70]PCBM in the matrix	%	22	27
W_I	Inner width of the region giving rise to $J_{\text{interface}}$	nm	11	11
W_O	Outer width of the region giving rise to $J_{\text{interface}}$	nm	4.5	4.5

3.2.3 Local contributions to the total photocurrent

Three different regions can be identified in the morphology depicted in Figure 3.1a. The inner-most part of the fullerene blob is not contributing to the photocurrent of the device, because the excitons that are there generated are not able to reach the donor/acceptor interface before decaying. The region around the blob, and far from its interface, is made of a mixture of polymer and fullerene; there the dissociation of excitons is efficient, and free electrons and holes are generated. They have to be extracted from the device, and their transport occurs entirely through the mixed phase. As shown in the previous chapter, the transport of the electrons in the mixed phase is not efficient, and this limits the current coming out from this region.

A third region exists in proximity of the interface of the fullerene blob, extending a few nanometres inside (W_I) and outside (W_O). The excitons generated inside the blob and within their diffusion distance from the interface can reach it and be dissociated. This dissociation yields free charges in different phases: the electron stays on the [70]PCBM molecules of the blobs, and travels through them towards the cathode; the hole is transferred to the polymer and transported through the mixed phase. The dissociation of the excitons generated close to the interface of the blob, but outside it, occurs into the mixed phase. But in this case the generated free electron is close enough to the [70]PCBM blob to diffuse towards it and then it is transported to the cathode through the acceptor phase. Thus, the excitons generated in this third region, even though for different reasons depending on where the generation took place, yields free carriers travelling through different phases.

The three regions described above are graphically shown in Figure 3.1b. The free holes generated at the bottom surface of the blobs, close to the anode, are easily extracted; the free electrons move vertically to the fullerene blobs and are then efficiently transported to the cathode. Thus, the region at the bottom of the blobs is considered to be part of the third region described above. The region at the top of the blobs is instead not considered: the holes that are generated in that area should travel laterally for a long distance along the top surface of the blobs, prior to be transported vertically to the anode through the matrix. We assume that these holes recombine before performing such a long lateral movement. The device can be described as the parallel connection of the second and the third region: the total current is therefore given by the sum of two separate contributions. We call J_{mixed} the current coming from the mixed-only region, and $J_{\text{interface}}$ the one coming from the interfacial region. Thus,

$$J_{\text{total}} = J_{\text{mixed}} + J_{\text{interface}}. \tag{3.1}$$

J_{mixed} is the current that we would extract from a mixed-phase only solar cell with low concentration of [70]PCBM. $J_{\text{interface}}$ is the current that we would get if the fullerene blobs were so small and densely packed to have a 100% efficient exciton dissociation and electron transport only through the acceptor phase. Both J_{mixed} and $J_{\text{interface}}$ can be calculated using the 1D drift-diffusion code, because they represent the current of devices in which the characteristic segregation length is much smaller than the thickness

of the active layer. We use an optical model (Section 3.3) to calculate the profile of the generation rate of excitons for the two regions giving rise to J_{mixed} and $J_{\text{interface}}$. We multiply these profiles for the volume fraction of the two regions and we use them as input for the calculation of the JV characteristics.

3.3 Optical modelling

When bulk heterojunction solar cells are fabricated with the device structure described in Section 1.6, the light comes into the device through the anode. It is therefore reasonable to assume that most of the light is absorbed close to the anode, which means that most of the charge carriers inside the active layer are generated close to the hole-collecting electrode.

As reported in the previous chapter, if the blend contains a significant amount of [70]PCBM the mobility of electrons matches the mobility of holes. If the charge transport is balanced, the electrical modelling of the cell can be done approximating the generation profile with a constant shape throughout the active layer; the same holds for systems in which electrons are faster than holes.[5] But for systems in which the electrons are significantly slower than the holes, as the blend PDPP5T:[70]PCBM 4:1 wt. ratio, it is not possible to neglect the fact that most of the electrons have to travel for a bigger distance than most of the holes in order to exit the device. For this blend, approximating the generation profile with a constant shape would lead to an underestimation of the recombination of charges within the active layer (see next Section).

The calculation of the optical profile of polymer solar cells is based on the transfer matrix model.[6–8] To correctly simulate the propagation and absorption of light through the stack of thin layers that compose the device, the reflectance of the top electrode and the interference effects need to be considered. We use a numerical code[5] to calculate the profile of exciton generation in the active layer of the solar cells made with the PDPP5T:[70]PCBM blends, with different polymer/fullerene ratios. The input parameters for this simulation are the thickness and the optical constants n and k of each layer of the device. The value of n and k for the pristine [70]PCBM and the PDPP5T:[70]PCBM blend 4:1 wt. ratio from chloroform are determined with variable angle ellipsometry on films cast on silicon substrates, using a Woollam VASE ellipsometer. The optical constants of the blends and the results of the simulation are shown in Figure 3.2. The 1D drift-diffusion model that we use[1] considers the excitons to be dissociated with an efficiency of unity. Therefore, the free charge generation profile used as input for the simulation of the JV curves corresponds to the exciton generation profile calculated with the transfer matrix approach.

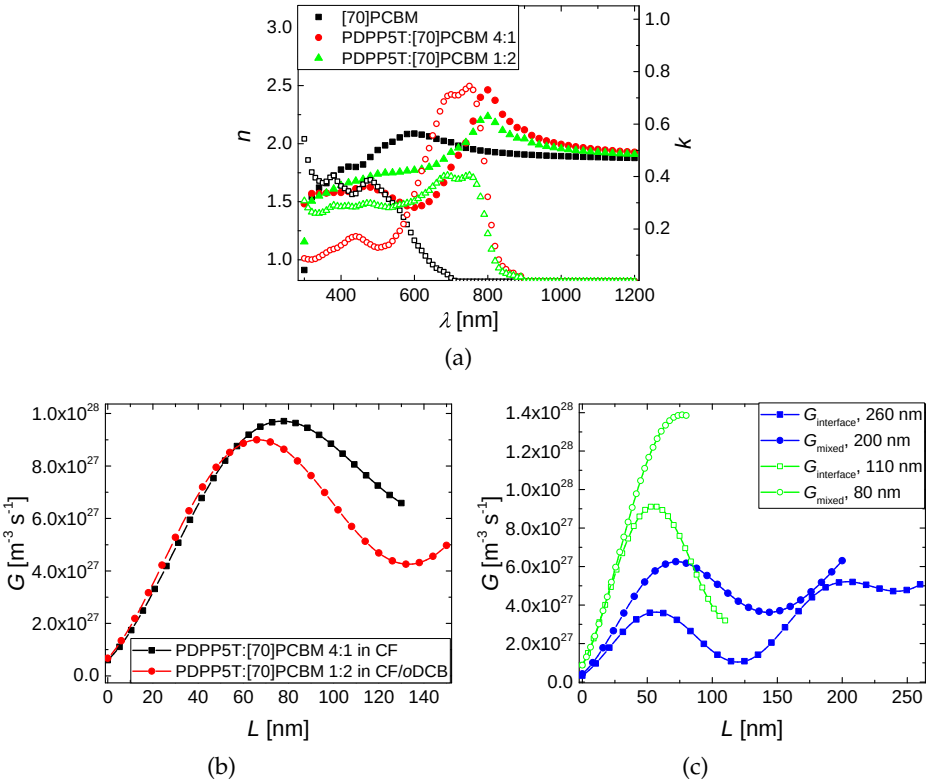

Figure 3.2: a) Optical constants n (full symbols) and k (empty symbols) for the pristine [70]PCBM and for the blends PDPP5T:[70]PCBM 4:1 wt. ratio spin cast from chloroform and PDPP5T:[70]PCBM 1:2 wt. ratio spin cast from chloroform/*o*DCB.

For the devices with coarse phase separation, we calculate two generation profiles: one for the generation of excitons at the interface of the fullerene blobs ($G_{\text{interface}}$), using the optical constants of pristine [70]PCBM; the other for the generation of excitons into the mixed phase (G_{mixed}), using the optical constants of the PDPP5T:[70]PCBM 4:1 wt. ratio blend. These two profiles are used to determine how many excitons contribute to each of the two currents that add up to give the total photocurrent.

3.4 Outcome of the simulations

We use the models described in Section 3.2.1 to fit the experimental JV characteristics of the solar cells made with the PDPP5T:[70]PCBM blends. The solar cells with a homogeneous active layer are simulated directly with the 1D model; for the solar cells with

a morphology characterized by a coarser phase separation, Equation 3.1 is used after simulating the two contributions to the total current with the 1D model.

3.4.1 Homogeneous devices

Figure 3.3 shows the fits of the homogeneous devices. The input parameters used to simulate the data with the 1D model are listed in Table 3.2.

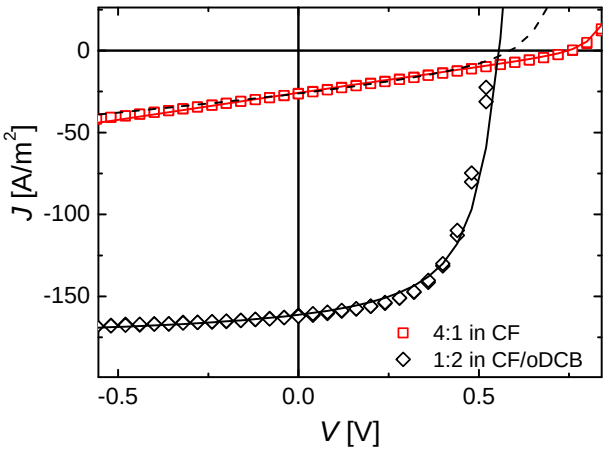

Figure 3.3: Experimental (symbols) and simulated (solid lines) JV curves for PDPP5T:[70]PCBM solar cells 4:1 wt. ratio cast from chloroform and 1:2 wt. ratio cast from chloroform/*o*DCB. To prove that the generation profile of charges has to be taken into account for the 4:1 blend, we perform the calculations using the same parameters and a constant profile. The resulting JVs is represented by a dashed line.

Table 3.2: Fit parameters for the simulation of the JV curves of the devices with homogeneous active layer.

Parameter	Units	PDPP5T:[70]PCBM 4:1 in CF	PDPP5T:[70]PCBM 1:2 in CF/*o*DCB
μ_n	$m^2\ V^{-1}\ s^{-1}$	6.8×10^{-12}	3.0×10^{-7}
γ_n	$m^{1/2}V^{-1/2}$	4.5×10^{-4}	0.5×10^{-4}
μ_p	$m^2\ V^{-1}\ s^{-1}$	3.2×10^{-7}	3.2×10^{-7}
γ_p	$m^{1/2}V^{-1/2}$	-4.8×10^{-4}	-4.8×10^{-4}
γ_{pre}	-	1	0.77
G	$\#\ m^{-3}\ s^{-1}$	9.7×10^{27}	9.07×10^{27}

The large difference between the performance of the two devices is related to the difference in electron mobility: as shown in Figure 2.6, upon increasing the amount of [70]PCBM in the blend, an enhancement of the zero-field electron mobility is obtained. The absolute values of the mobility with different [70]PCBM content, however, are not enough to explain the shape of the JV characteristics obtained for the PDPP5T:[70]PCBM 4:1 wt. ratio solar cell. According to the space charge theory,[9] and considering the electrons to be the slowest carriers, the maximum allowed photocurrent J_{ph} would be:[10]

$$J_{ph} = \left(\frac{9\varepsilon\mu_n}{8}\right)^{1/4} (qG)^{3/4} V_{\text{eff}}^{1/2}. \tag{3.2}$$

Here, V_{eff} is the effective applied voltage, given by $V_0 - V$. V_0 is the compensation voltage, at which $J_{ph} = 0$; V is the applied voltage.

According to Equation 3.2, the photocurrent would follow a $1/2$ power dependence on the voltage, and the JV would have the shape of a parabola, with a FF around 42%.[9] The outcome of our experiment is instead a straight JV characteristics in reverse bias, with a FF around 29%.

The difference between theory and experiment is due to the electric field dependency of the electron mobility. Consider a bulk heterojunction solar cell in which the photogeneration of holes and electrons is uniform throughout the thickness of the active layer. If the transport is unbalanced, electrons and holes will have different drift lengths $w_{n(p)} = \mu_{n(p)}\tau_{n(p)}F$, $\tau_{n(p)}$ being the charge carrier lifetime. If one or both the drift lengths are smaller than the thickness L of the active layer, space charge will form. In the case of PDPP5T:[70]PCBM system with low [70]PCBM content, $w_n \ll w_p$ and $w_n < L$: the electrons accumulate in the active layer, modifying the internal electric field. This increases in the region L_1 close to the cathode, enhancing the extraction of electrons. A steady state is reached when the extension of L_1 is such to have an external electron current which equals the external hole current. The length of the region in which space charge is accumulated is given by the electron drift length. Most of the voltage drops in the active layer occurs in the region L_1, so that $V_1 \approx V$ and the total photocurrent corresponds to the photocurrent generated in the region L_1:

$$J_{ph} = qGL_1. \tag{3.3}$$

Goodman and Rose showed that the electrostatic limit for the build-up of space charge is reached when the extracted photocurrent is equal to the space charge limited current.[10] Assuming a Poole-Frenkel dependence on the electric field for the electron mobility (Equation 2.3), the space charge limited current J_{SCL} is approximated by[11]

$$J_{\text{SCL}} = \frac{9}{8}\varepsilon\mu_o \exp\left(0.891\gamma\sqrt{\frac{V_{\text{eff}}}{L}}\right), \frac{V_{\text{eff}}^2}{L^3}. \tag{3.4}$$

where γ is the field activation factor. Equating J_{ph} and J_{SCL}, the thickness of the region in which the space charge is built up is found:

$$L_1 = \left(\frac{9\varepsilon\mu_n V^2}{8qG}\right)^{1/4} \exp\left(0.222\gamma\sqrt{\frac{V}{L}}\right). \tag{3.5}$$

Substituting this in Equation 3.3 yields the maximum electrostatically allowed photocurrent:

$$J_{ph} = \left(\frac{9\varepsilon\mu_n}{8}\right)^{1/4} \exp\left(0.222\gamma\sqrt{\frac{V}{L}}\right) (qG)^{3/4}\, V^{1/2}. \tag{3.6}$$

For $\gamma = 0$, the photocurrent is the same derived for space charge limited photocurrent with field-independent carrier mobility (Equation 3.2).

Equation 3.6 is more suitable to describe the experimental data. A comparison of the photocurrent calculated using Equation 3.2 and 3.6 is shown in Figure 3.4. As discussed in Section 3.3, the generation profile of charge carriers has to be included in order to model the JV characteristics of the device; Equation 3.6 cannot therefore be used directly to fit the experimental data.

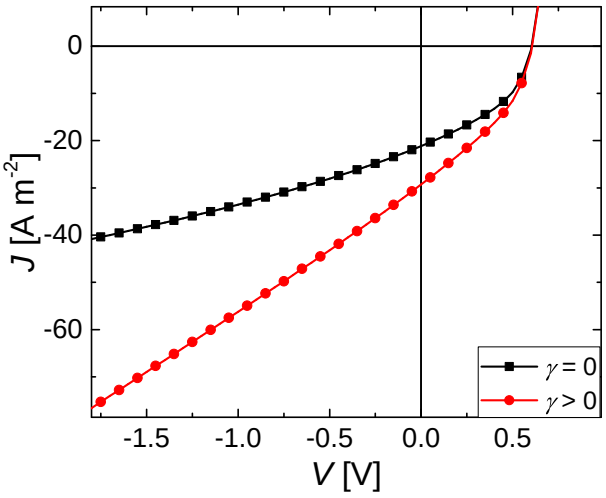

Figure 3.4: JV characteristics of a polymer:fullerene solar cell with space charge limited current, calculated using Equation 3.6 with and without electric field dependency for the electron mobility. The curves in the plot are obtained by subtracting J_{ph} from the dark current. For both the curves, the dark current is simulated with the parameters reported in Table 3.2 for the PDPP5T:[70]PCBM device, setting $G = 0$.

If the mobility of electrons gets close to the mobility of holes, the space charge limit is eliminated and the JV characteristic becomes less field-dependent, giving a flat curve in reverse bias. As a consequence of this, the device based on the PDPP5T:[70]PCBM 1:2 wt. ratio blend cast from chloroform/*o*DCB exhibits a great enhancement of efficiency if compared to the homogeneous device with low [70]PCBM content.

3.4.2 Phase-separated devices

The addition of *o*DCB as a co-solvent to the blend PDPP5T:[70]PCBM 1:2 wt. ratio has an effect on the morphology: with this amount of fullerene in the blend and without co-solvent, a phase-separated morphology (Figure 2.3c and d) is obtained.

The fits of the phase-separated blends are displayed in Figure 3.5, and the parameters are listed in Table 3.3.

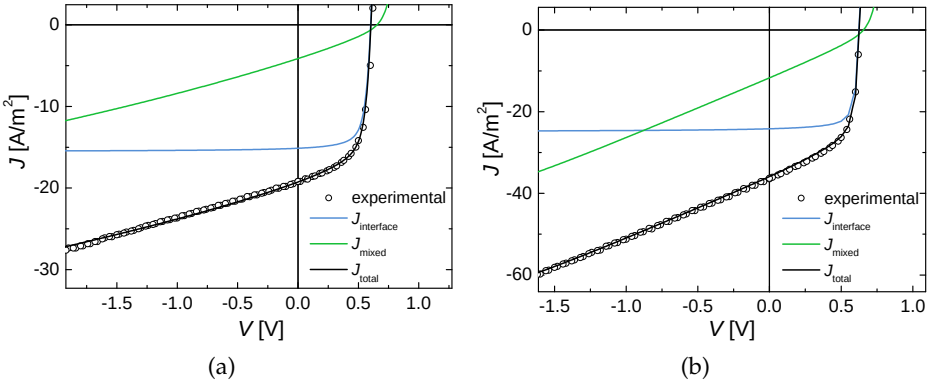

Figure 3.5: Experimental and simulated J-V curves for PDPP5T:[70]PCBM solar cells: (a) 1:2 wt. ratio cast from chloroform, 260 nm thick; (b) 1:2 wt. ratio cast from chloroform, 110 nm thick.

For both devices, before simulating the two contributions J_{mixed} and $J_{\text{interface}}$, we need to determine which exciton generation rates have to be used as input for the two simulations. First, the profiles of exciton generation for the mixed and the acceptor phase are calculated with a transfer matrix approach. For the mixed and the acceptor phase, we use the optical constants of the blend PDPP5T:[70]PCBM 4:1 wt. ratio and of pristine [70]PCBM, respectively. The exciton generation profiles are then multiplied by the volume fraction of the two regions from where J_{mixed} and $J_{\text{interface}}$ come. The volume fractions depend on the geometrical parameters utilized to mimic the morphology and on the width of the region around the interface of the blobs, inside and outside (W_I and W_O). These latter values represent fit parameters; remarkably, for both the devices the same values of W_I and W_O were used to fit the experimental data, i. e. W_I = 11 nm and

Table 3.3: Fit parameters for the simulation of the JV curves of the devices with coarse phase separation in the active layer.

Parameter	Units	Thick device	Thin device
		$J_{\mathbf{mixed}}$	
μ_n	$m^2\ V^{-1}\ s^{-1}$	5.4×10^{-12}	9.8×10^{-12}
γ_n	$m^{1/2}V^{-1/2}$	1.1×10^{-4}	2.9×10^{-4}
μ_p	$m^2\ V^{-1}\ s^{-1}$	3.2×10^{-7}	3.2×10^{-7}
γ_p	$m^{1/2}V^{-1/2}$	-4.8×10^{-4}	-4.8×10^{-4}
γ_{pre}	-	1	1
G	$\#\ m^{-3}\ s^{-1}$	3.12×10^{27}	7.14×10^{27}
		$J_{\mathbf{blob}}$	
μ_n	$m^2\ V^{-1}\ s^{-1}$	2.0×10^{-7}	2.0×10^{-7}
γ_n	$m^{1/2}V^{-1/2}$	0.5×10^{-4}	0.5×10^{-4}
μ_p	$m^2\ V^{-1}\ s^{-1}$	3.2×10^{-7}	3.2×10^{-7}
γ_p	$m^{1/2}V^{-1/2}$	-4.8×10^{-4}	-4.8×10^{-4}
γ_{pre}	-	0.05	0.1
G	$\#\ m^{-3}\ s^{-1}$	6.18×10^{26}	2.11×10^{27}

W_O = 4.5 nm. The asymmetry of this region around the interface is due to the different physical phenomena occurring inside and outside the blob. Inside, the excitons, neutral species, are diffusing towards the interface, where they are dissociated. Outside, the dissociation of excitons in the mixed phase precedes the lateral motion of electrons towards the acceptor phase.

For both phase-separated active layers, most of the current at the maximum power point (around 0.53 V) comes from the blob interfaces. Also at short circuit conditions, $J_{\text{interface}}$ represents more than 70% of the total current. This means that in forward bias most of the free charges generated far from the blobs are not extracted from the device, and undergo bimolecular recombination. J_{mixed} becomes important in the high reverse bias region, in which the electric field favours the vertical movement of electrons towards their collecting electrode. In the active layer with smaller blobs, more fullerene is dispersed into the polymer matrix. The mobility of electrons is thus high if compared to the electron mobility in the mixed phase of the other device. This causes a shift of the crossing point between J_{mixed} and $J_{\text{interface}}$ towards smaller reverse bias, because a less strong field is required for the vertical transport of electrons to take place into the mixed phase.

It should be noted that the relative importance of the two currents is dependent on material properties and on the morphology. For the devices presented here, most of the photocurrent in forward bias comes from the interfacial region between the blobs and the matrix. The same conclusion arises from local photocurrent analysis performed

by Pingree *et al.* on polymer:fullerene systems with similar morphology through photoconductive AFM (pc-AFM).[12] Other pc-AFM data show instead local variations of photocurrent which are not correlated with the blob presence and with extends on much longer lengthscales than the size of the fullerene aggregates.[13,14] We therefore assume that analysing other systems with the parallel approach would yield different results.

The parameters in Tables 3.1 and 3.3 also explain why J_{sc} and FF of the thicker device are lower than the current of the thinner device. Beside having a lower extent of donor:acceptor interface, which translates into a less efficient dissociation of excitons (*i. e.* a lower G), the thicker device has also a lower concentration of [70]PCBM in the mixed phase. This means that the electron mobility in the mixed phase of the thicker device is lower than in the mixed phase of the thinner device. Hence, J_{mixed} is more steep for the thicker device, resulting in a lower FF. These results are in agreement with what reported by Kouijzer *et al.* , who proposed that the change of [70]PCBM concentration in the matrix causes a change in the shape of the JV curve.[2]

3.5 Conclusion

The efficiency of the solar cell made with the blend PDPP5T:[70]PCBM 4:1 wt. ratio is strongly limited by i) the poor electron mobility, giving rise to space charge, and ii) the dependency of μ_n on the electric field, further reducing FF. These limits are not present in the device made of PDPP5T:[70]PCBM 1:2 wt. ratio spin cast from a chloroform/*o*DCB solutions. These two devices have homogeneous active layers, in which the polymer and the fullerene are mixed with a segregation length smaller than the diffusion length of excitons and much smaller than the thickness of the devices. Thus, it is possible to simulate the JV characteristics of the devices directly, using the 1D code.

A different approach is necessary to model the JV curves of the devices with coarse phase separation in the active layer. Spin casting of the blend PDPP5T:[70]PCBM from a chloroform solution yields an active layer with large fullerene domains dispersed into a polymer-rich matrix. Both the size of the domains and the composition of the matrix vary with the evaporation time. The total current extracted from these devices is modelled as the sum of two contribution: one, due to charge carriers travelling entirely through the mixed phase, is space charge limited, because the mobility of electrons in the mixed phase is several order of magnitudes smaller than the mobility of holes; the other, coming from the region close to the interface of the blobs, is the result of a balanced transport (holes carried by the mixed phase, electrons travelling through the acceptor phase). In order to calculate the two contributions, we estimated how many excitons are generated close to the interface, and how many are lost for not being able to reach it (the excitons generated inside the blobs and too far from the interface). Remarkably, a reduction of the Langevin recombination strength is observed in case of coarse phase separation (Chapter 2); therefore, we model the contribution of current from the mixed phase with a recombination prefactor equal to unity, and we reduce it to model the contribution of the interfacial region.

Interestingly, at the maximum power point of the device most of the total current turns out to come from the interfacial region, even though most of the excitons generated into the active layer contribute to the other current. Only at high reverse bias did the contribution of the mixed phase become predominant; nevertheless, its presence is also important in forward bias, since it determines the shape of the curve, and hence the fill factor of the solar cell. PDPP5T:[70]PCBM blends yield a wide range of morphologies, from finely dispersions to coarse phase-separated films. These morphologies can be controlled by varying the processing conditions, and are the same kind of morphology already observed in many other polymer:fullerene systems. Therefore, the model that we have here presented is potentially applicable to other systems.

References

[1] L. J. A. Koster, E. C. P. Smits, V. D. Mihailetchi, P. W. M. Blom, *Phys. Rev. B* **2005**, *72*, 085205.

[2] S. Kouijzer, J. J. Michels, M. van den Berg, V. S. Gevaerts, M. Turbiez, M. M. Wienk, R. A. J. Janssen,. *J. Am. Chem. Soc.* **2013**, *135*, 12057.

[3] W. Geens, T. Martens, J. Poortmans, T. Aernouts, , , J. Manca, L. Lutsen, P. Heremans, S. Borghs, R. Mertens, D. Vanderzande, *Thin Solid Films* **2004**, *451*, 98.

[4] K. Maturová, S. S. van Bavel, R. A. J. Janssen, M. Kemerink, *Nano Lett.* **2009**, *9*, 3032.

[5] J. D. Kotlarski, P. W. M. Blom, L. J. A. Koster, M. Lenes, L. H. Slooff, *Appl. Phys.* **2008**, *103*, 084502.

[6] Z. Knittl, *Optics of thin films*, Wiley, London, 2012.

[7] L. A. A. Petterson, L. S.Romans, O. Inganäs, *J. Appl. Phys.* **1999**, *86*, 487.

[8] P. Peumans, A. Yakimov, S. Forrest, *J. Appl. Phys.* **2003**, *93*, 3693.

[9] V. D. Mihailetchi, J. Wildeman, P. W. M. Blom, *Phys. Rev. Lett.* **2005**, *94*, 126602.

[10] A. M. Goodman, A. Rose, *J. Appl. Phys.* **1971**, *42*, 2823.

[11] P. N. Murgatroyd, *J. Phys. D Appl. Phys.* **1970**, *3*, 151.

[12] L. S. C. Pingree, O. G. Reid, D. S. Ginger, *Adv. Mater.* **2009**, *21*, 19.

[13] D. C. Coffey, O. G. Reid, D. B. rodovsky, G. P. Bartholomew, D. S. Ginger, *Nano Lett.* **2007**, *7*, 738.

[14] T. A. Bull, L. S. C. Pingree, S. A. Jenekhe, D. S. Ginger, C. K. Luscombe, *ACS Nano* **2009**, *3*, 627.